Supporting Information

Ultrathin, 2D PdAg alloy mesoporous nanosheets enriched with nanogaps promote electrocatalytic CO_2 reduction to formate

Shangqing Sun[#a], Miaomiao Liu[#b], Yalan Mao[a], Fang Liu[a], Xinyuan Xu[a], Yuan Li[a], Ximei Lv[a], Shulin Zhao[a], Xiaojing Liu [a]*, Yuping Wu[a,c], and Yuhui Chen[a]

[a] *State Key Laboratory of Materials-Oriented Chemical Engineering, School of Energy Science and Engineering, Nanjing Tech University, Nanjing 211816, China*

[b] *Key Laboratory of Interfacial Physics and Technology, Shanghai Institute of Applied Physics, Chinese Academy of Sciences, Jialuo Road 2019, Shanghai 201800, China*

[c] *Confucius Energy Storage Lab, School of Energy and Environment & Z Energy Storage Center, South East University, Nanjing, Jiangsu 211189, China*

[#] *S. Q. Sun and M. M. Liu contributed equally to this work.*

**Corresponding author: X. J. Liu. Email: xjliu022@njtech.edu.cn*

Table S1. ICP results of as-prepared PdAg samples with different precursor ratios.

Sample	Pd (at%)	Ag (at%)
Pd_1Ag_1	54.95	45.05
Pd_2Ag_1	65.99	34.01
Pd_4Ag_1	80.54	19.46

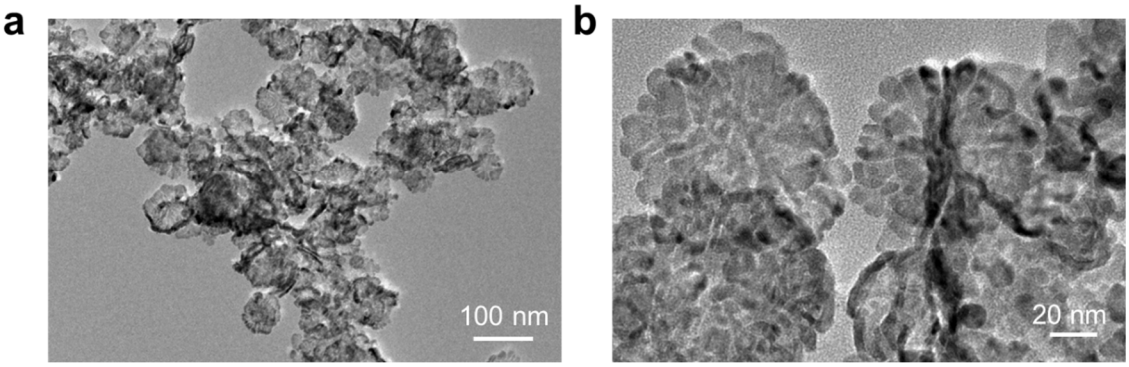

Figure S1. TEM images of Pd_4Ag_1 NSs.

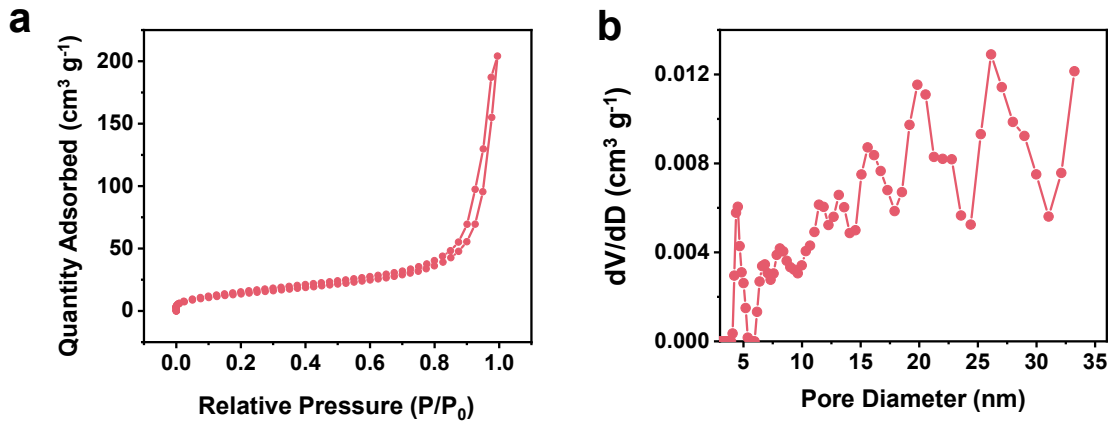

Figure S2. (a) Nitrogen adsorption−desorption isotherm, (b) the pore size distribution of Pd_4Ag_1 NSs.

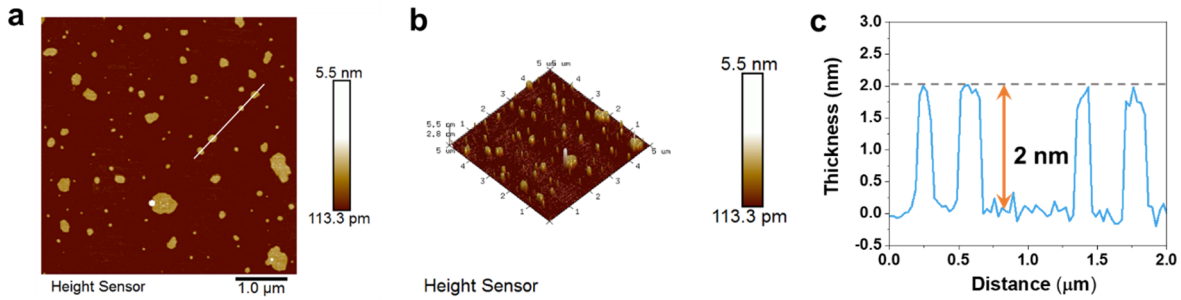

Figure S3. (a) AFM two-dimensional topographic image, (b) AFM three-dimensional topographic image and (c) thickness analysis of Pd_4Ag_1 NSs.

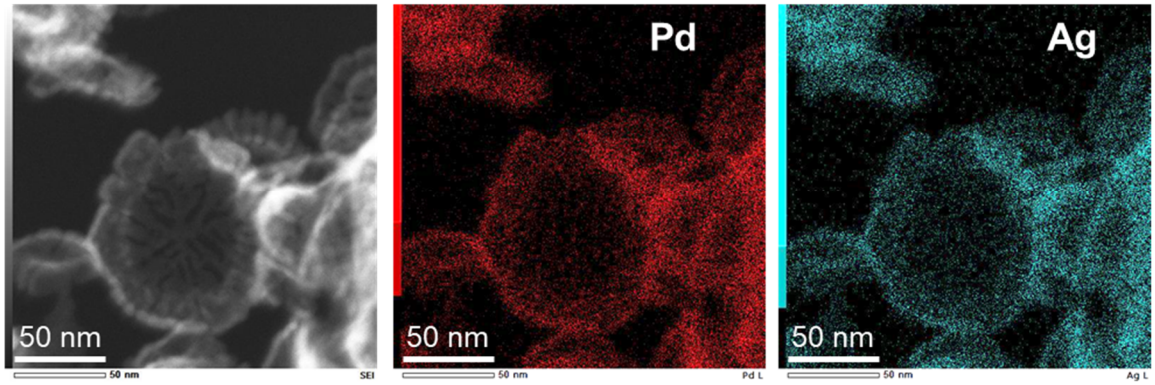

Figure S4. EDS elemental mapping images of Pd_4Ag_1 NSs.

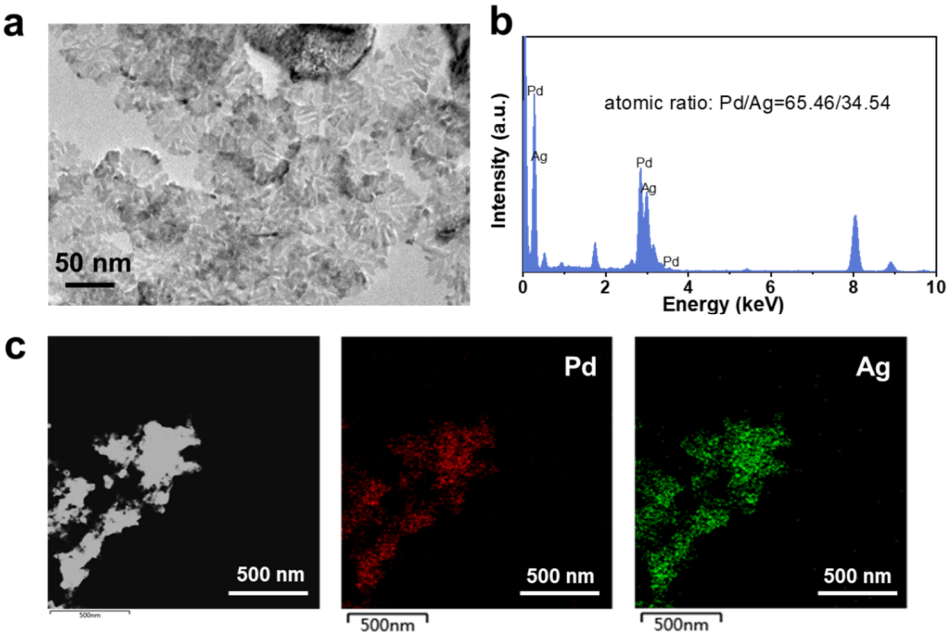

Figure S5. Structural characterizations of Pd_2Ag_1 NSs. (a) TEM image, (b) EDS spectrum, (c) EDS elemental mapping images.

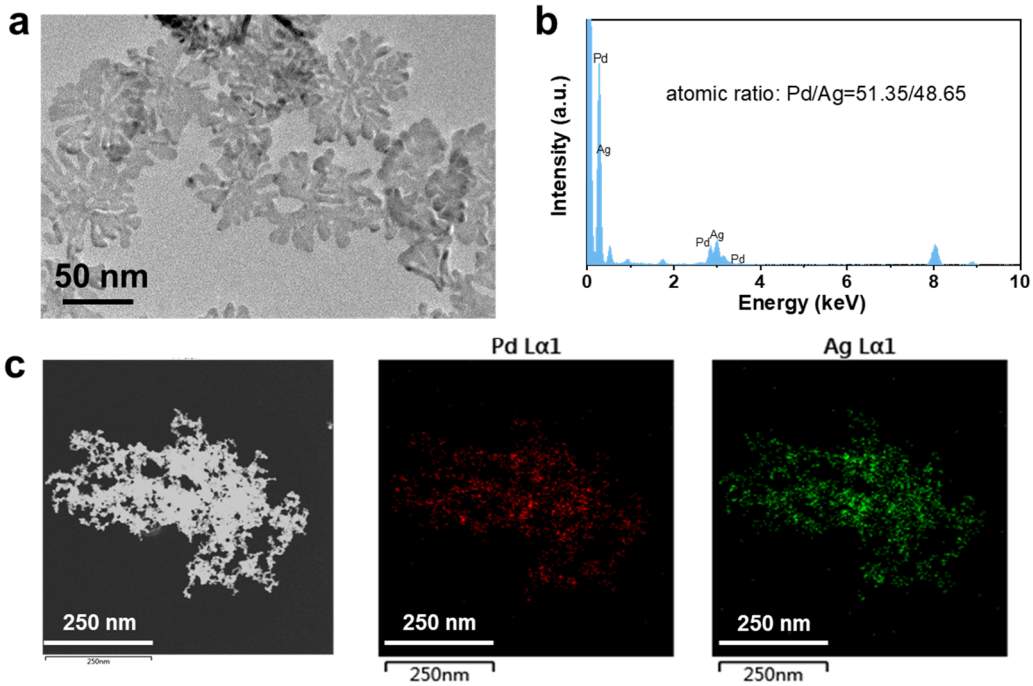

Figure S6. Structural characterizations of Pd_1Ag_1 NSs. (a) TEM image, (b) EDS spectrum, (c) EDS elemental mapping images.

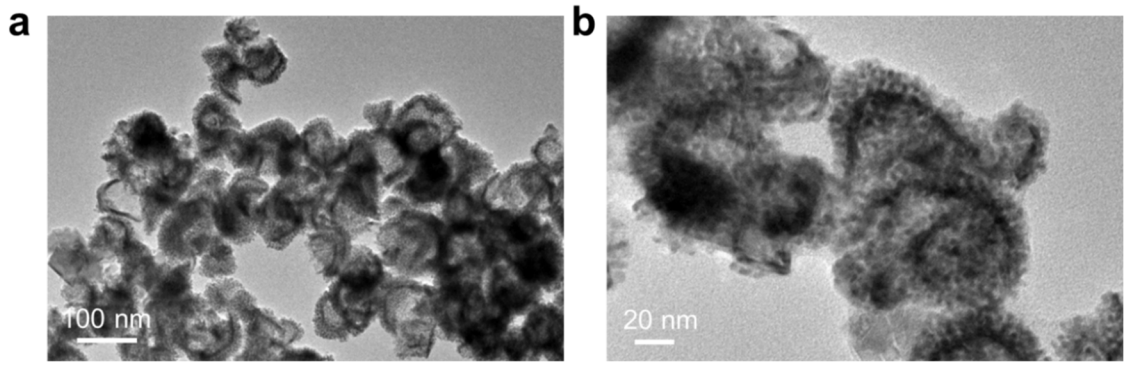

Figure S7. TEM images of pure Pd when C_{22}TAC was employed as a structure-directing agent.

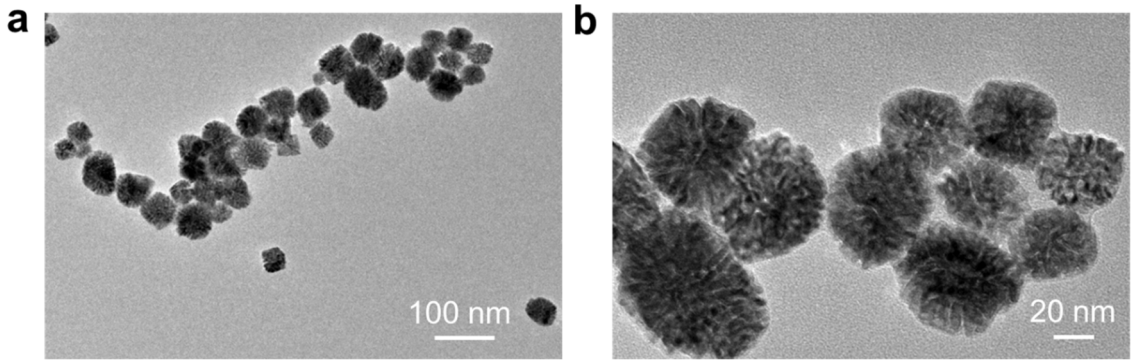

Figure S8. TEM images of pure Pd NCs when STAC was employed as a structure-directing agent.

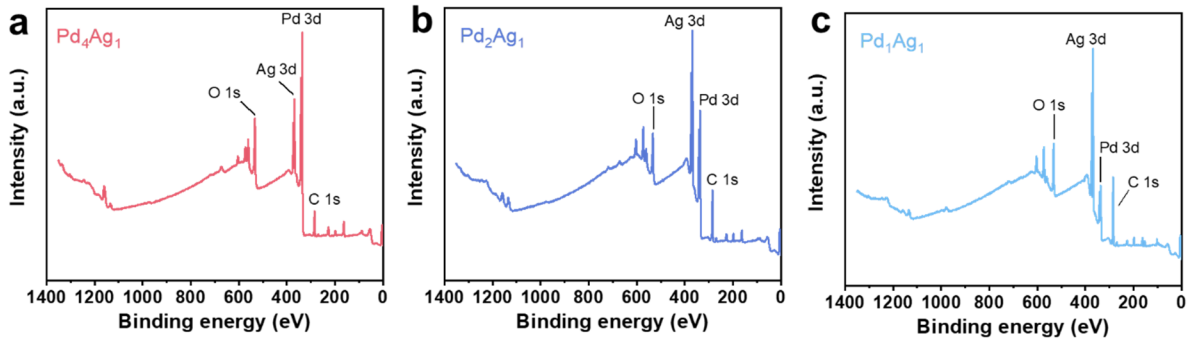

Figure S9. XPS overall survey spectra of (a) Pd_4Ag_1, (b) Pd_2Ag_1 and (c) Pd_1Ag_1 NSs.

Table S2. Fitting peak area of Pd 3d spectrum in Pd-based catalysts.

Sample	The area of Pd^0	The area of Pd^{2+}	The area of Pd^{4+}	The proportion of Pd^0 state of all samples
Pd_1Ag_1	45787.5	41459.6	44428.8	34.8%
Pd_2Ag_1	68008.1	151646.3	113300.2	20.4%
Pd_4Ag_1	86600.3	250394.9	316394.3	13.3%

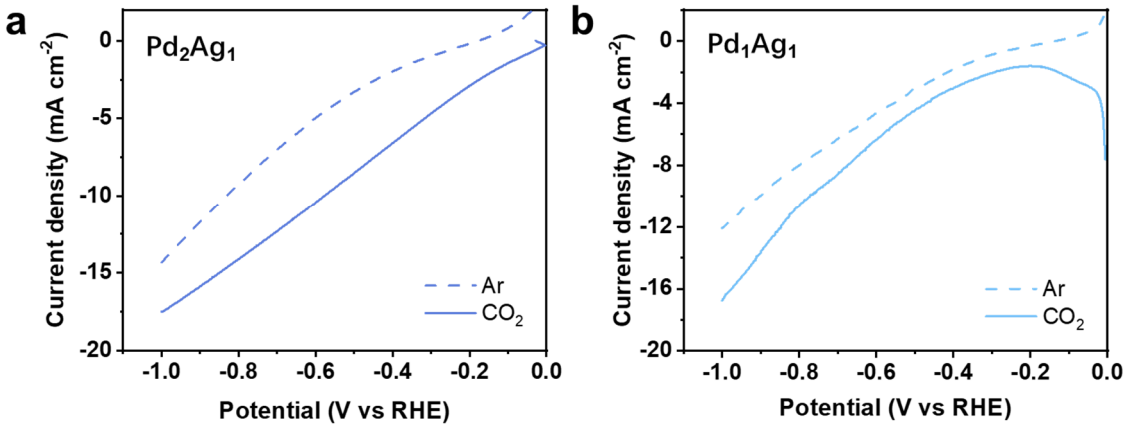

Figure S10. Polarization curves of (a) Pd_2Ag_1 and (b) Pd_1Ag_1 catalysts in Ar- or CO_2-saturated 0.1 M $KHCO_3$ aqueous electrolyte at a scan rate of 50 mV s^{-1}.

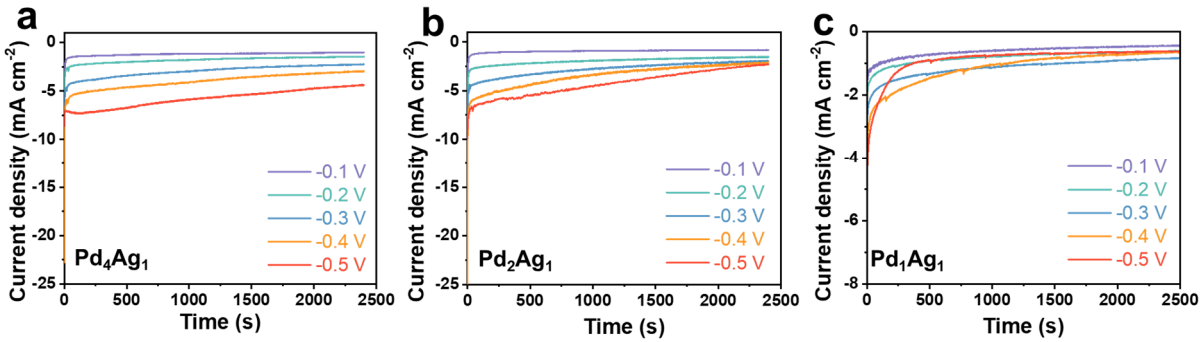

Figure S11. Chronoamperometry results of (a) Pd_4Ag_1, (b) Pd_2Ag_1 and (c) Pd_1Ag_1 catalysts at different applied potential in CO_2-saturated 0.1 M $KHCO_3$ solution.

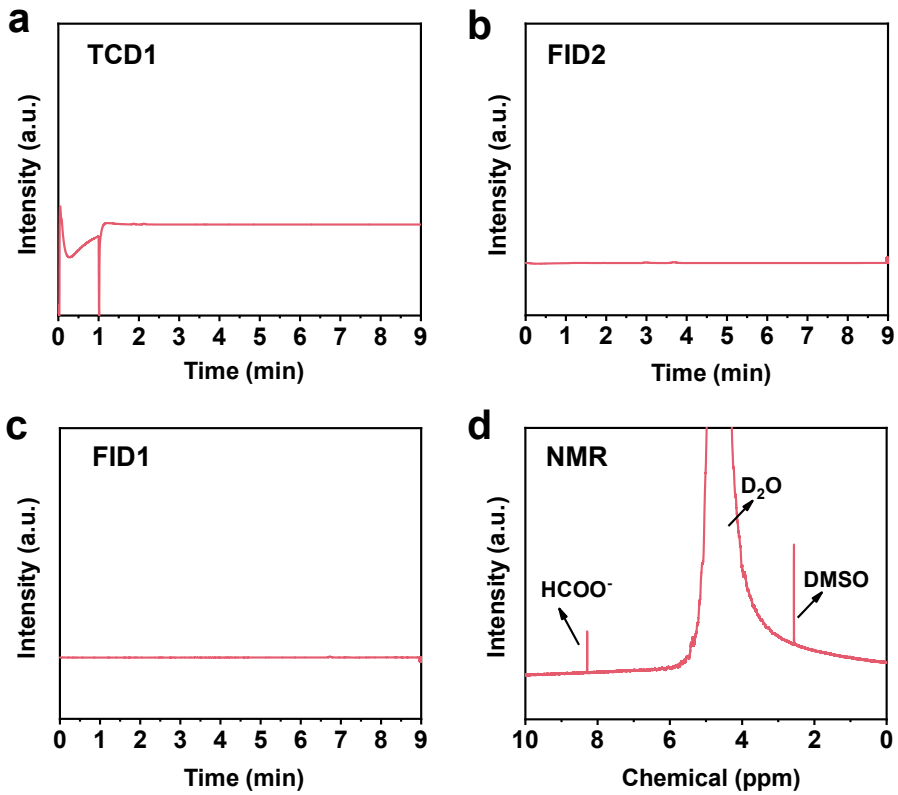

Figure S12. (a-c) GC spectra and (b) ^{1}H NMR spectrum of CO_2RR products obtained at the potential of –0.1 V on Pd_4Ag_1 NSs.

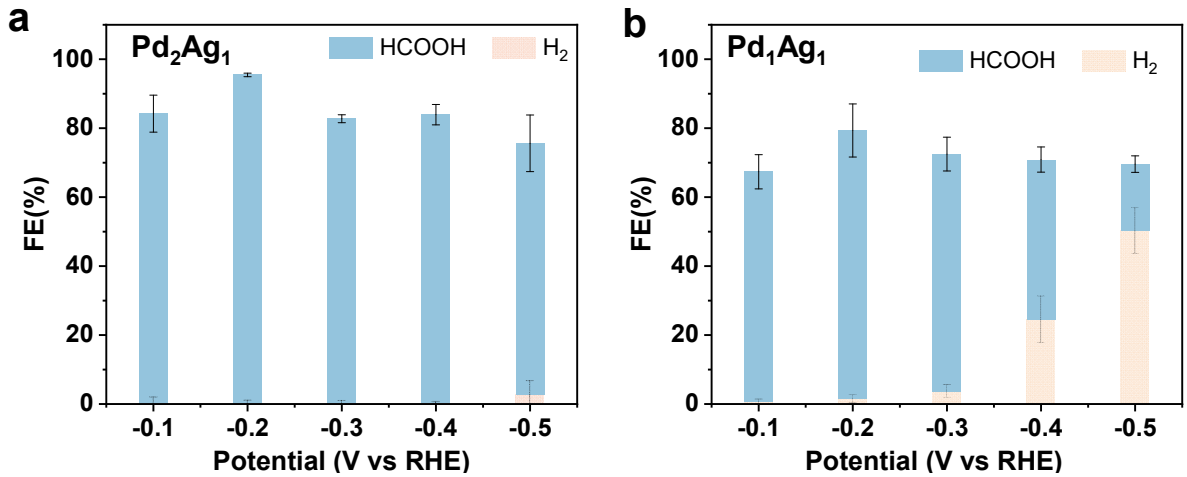

Figure S13. Potential-dependent faradaic efficiencies of various CO_2 reduction products on (a) Pd_2Ag_1 NSs and (b) Pd_1Ag_1 NSs catalysts at different potentials.

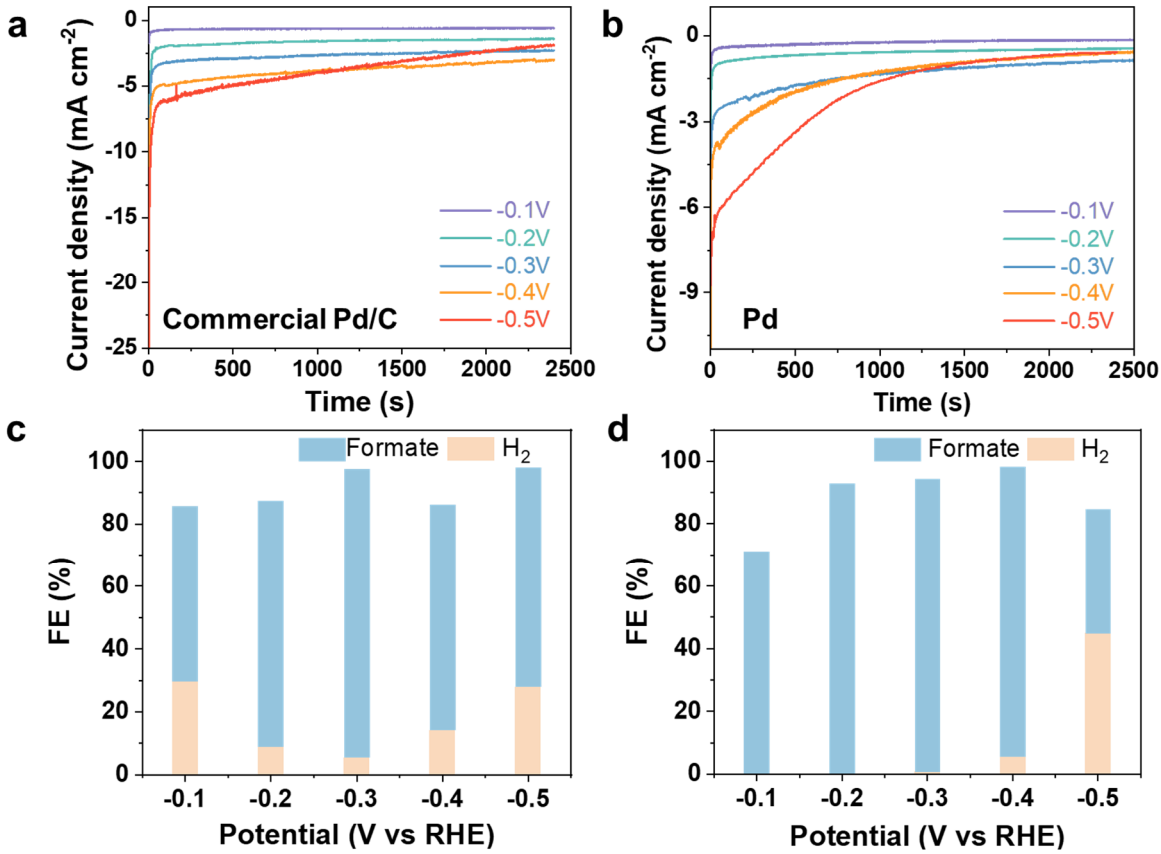

Figure S14. Chronoamperometry curves of (a) commercial Pd/C and (b) pure Pd NCs catalysts, potential-dependent faradaic efficiencies of (c) commercial Pd/C and (d) pure Pd NCs catalysts at different potentials.

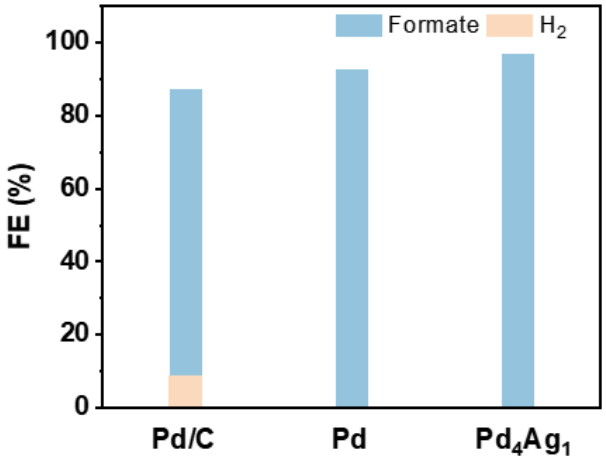

Figure S15. Comparison of formate faradaic efficiency for Pd-based catalysts at −0.2 V vs. RHE.

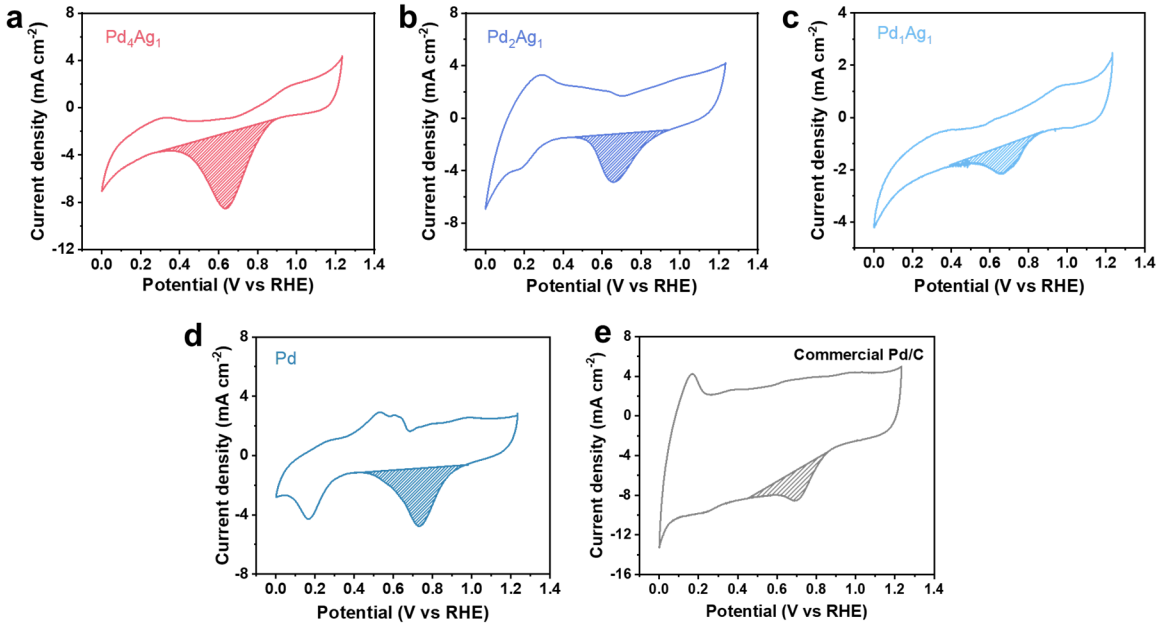

Figure S16. CV curves of (a) Pd_4Ag_1, (b) Pd_2Ag_1, (c) Pd_1Ag_1, (d) pure Pd and (e) commercial Pd/C catalysts in Ar-saturated 1 M KOH solution at a scan rate of 50 mV s^{-1}.

Table S3. ECSAs of Pd-based catalysts.

Sample	Pd mass loading (mg)	ECSA(m^2 g^{-1})
Pd/C	1	2.50
Pd	1	3.90
Pd_1Ag_1	0.5	4.49
Pd_2Ag_1	0.67	5.43
Pd_4Ag_1	0.80	9.27

Table S4. Performance comparison of representative Pd-based electrocatalysts for CO_2 reduction to formic acid/formate.

Electrocatalysts	Electrolytes	Potential at FE_{max} (V vs. RHE)	FE_{max} (%)	Stability	Reference
Pd_4Ag_1 NSs	0.1 M $KHCO_3$	–0.1	99.4	220 min	This work
6.8 nm Pd NPs	0.5 M $NaHCO_3$	–0.1	98	≈3600 s	[1]
s-mesoPdCu	0.1 M $KHCO_3$	–0.1	≈100	15000 s	[2]
Pd-B/C	0.1 M $KHCO_3$	–0.5	70	2 h	[3]
PdAg_2	0.1 M $NaHCO_3$	–0.27	94	10000 s	[4]
M-AuPd(20)	0.5 M $KHCO_3$	–0.25	＞99	3600 s	[5]

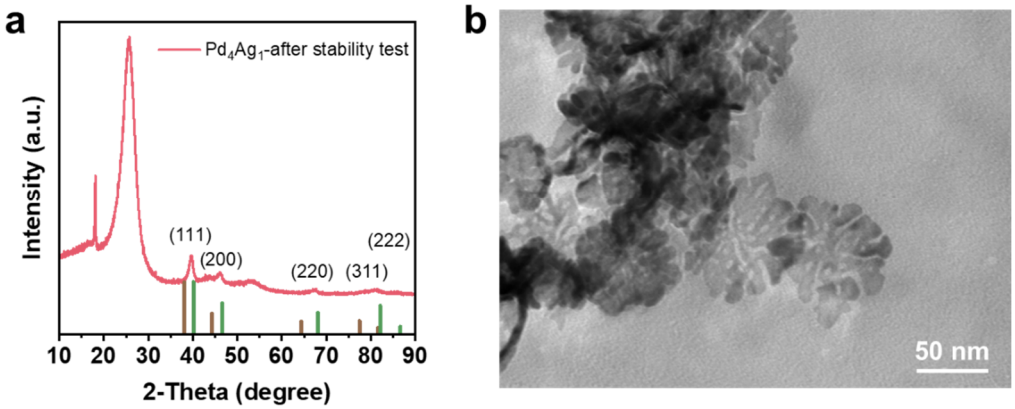

Figure S17. (a) XRD and (b) TEM image of Pd_4Ag_1 NSs after the stability test.

References

[1] M. Rahaman, A. Dutta and P. Broekmann, Size-Dependent Activity of Palladium Nanoparticles: Efficient Conversion of CO_2 into Formate at Low Overpotentials, ChemSusChem, 2017, 10, 1733-1741.

[2] H. Lv, F. Lv, H. Qin, X. Min, L. Sun, N. Han, D. Xu, Y. Li and B. Liu, Single-Crystalline Mesoporous Palladium and Palladium-Copper Nanocubes for Highly Efficient Electrochemical CO_2 Reduction, CCS Chem., 2022, 4, 1376-1385.

[3] B. Jiang, X.-G. Zhang, K. Jiang, D.-Y. Wu and W.-B. Cai, Boosting Formate Production in Electrocatalytic CO_2 Reduction over Wide Potential Window on Pd Surfaces, J. Am. Chem. Soc., 2018, 140, 2880-2889.

[4] Y. Zhou, R. Zhou, X. Zhu, N. Han, B. Song, T. Liu, G. Hu, Y. Li, J. Lu and Y. Li, Mesoporous PdAg Nanospheres for Stable Electrochemical CO_2 Reduction to Formate, Adv. Mater., 2020, 32, 2000992.

[5] J. Bok, S. Y. Lee, B. -H. Lee, C. Kim, D. L. T. Nguyen, J. W. Kim, E. Jung, C. W. Lee, Y. Jung, H. S. Lee, J. Kim, K. Lee, W. Ko, Y. S. Kim, S. -P. Cho, J. S. Yoo, T. Hyeon and Y. J. Hwang, Designing Atomically Dispersed Au on Tensile-Strained Pd for Efficient CO_2 Electroreduction to Formate, J. Am. Chem. Soc., 2021, 143, 5386-5395.